JAAS

ROYAL SOCIETY OF CHEMISTRY

PAPER

View Article Online
View Journal | View Issue

Cite this: *J. Anal. At. Spectrom.*, 2022, **37**, 1063

Validating the high-precision measurement of Mo isotopes at the 5 ng level using double spike MC-ICP-MS†

Hong-Gang Zhu, [a] Jian-Ming Zhu, *[a] Decan Tan, [b] Xuan Lin,[a] Kaite Lu[a] and Wen Yang[a]

With recent advancements in analytical methods of Mo isotopes, the $\delta^{98/95}$Mo ratios of most geological and environmental samples can be determined. Still, it remains a challenge to obtain high-precision Mo isotope data for low-Mo samples with complex matrices such as igneous and plant samples. Here, we present an improved Mo purification and cleaning resin scheme for reducing the total procedure blank to ≤0.16 ng using common Muromac®1X8(AG1-X8) anion and AG50-X8 cation resins. By an improved Aridus II with ice chamber in sample introduction system (SIS) and adding nitrogen (N_2), high sensitivity measurement (^{95}Mo signal intensity: 200–330 V ppm^{-1}) of Mo isotopes was achieved on Neptune Plus MC-ICP-MS. Thus, the sample size containing 30–60 ng Mo is sufficient to be purified, and isotope measurement with high-precision (≤0.06‰, 2SD) can be determined at a concentration of 3–10 ng level using a ^{97}Mo–^{100}Mo double spike. NIST 3134 (0.00 ± 0.05‰), SGR-1b (0.41 ± 0.05‰), NOD-P-1 (−0.86 ± 0.03‰), IAPSO (2.07 ± 0.04‰), and other international reference materials (RMs) were analyzed at 3, 5, 10, and 20 ng mL^{-1} levels to be in excellent agreement with the published $\delta^{98/95}$Mo values, demonstrating that good accuracy and precision of Mo isotope analysis can be achieved with an injecting sample size as small as 5 ng Mo. Our improved method can be applied to various geological and environmental samples. The $\delta^{98/95}$Mo of CLB-1 (1.25 ± 0.03‰), JDO-1 (0.50 ± 0.02‰), GSV-2 (0.47 ± 0.02‰), and other 38 RMs with relatively higher and lower Mo concentrations are reported for the first time. The total average $\delta^{98/95}$Mo ratio of 8 soils and 18 sediments is 0.003 ± 0.277‰ (1SD, n = 26), slightly lighter than that of the upper continent crust (0.05–0.15‰). The $\delta^{98/95}$Mo ratios (0.23–0.79‰, n = 8) of plant and animal origins from the land show they are enriched in heavy isotopes relative to the bulk silicate earth (BSE). The $\delta^{98/95}$Mo ratios of carbonates are much lower than that in seawater.

Received 28th December 2021
Accepted 18th March 2022

DOI: 10.1039/d1ja00465d

rsc.li/jaas

1. Introduction

Molybdenum (Mo) is a redox-sensitive element existing in two predominant valence states (Mo(IV) and Mo(VI)) in the natural environment. It has seven stable isotopes, ^{92}Mo (14.65%), ^{94}Mo (9.19%), ^{95}Mo (15.87%), ^{96}Mo (16.67%), ^{97}Mo (9.58%), ^{98}Mo (24.29%), and ^{100}Mo (9.74%), respectively.[1] The transformation between the different Mo oxidation states or Mo species is always related to Mo isotope fractionation. The considerable variation of $\delta^{98/95}$Mo values has been found in black shales, organic-rich mudrocks, crustal sulfide minerals, and manganese nodules with the whole range of ~5.5‰.[2–6] Consequently, molybdenum isotope systematics has become a powerful proxy in reconstructing the evolution of palaeo-atmosphere/ocean oxygenation,[7–9] redox condition of the modern ocean[10–13] and lake,[3] and in identifying the origin of hydrogenous and hydrothermal ferromanganese crusts or nodules.[14] Recently, the application of Mo isotopes to igneous rocks has revealed Mo isotope fractionation with up to 2‰,[15–20] demonstrating that Mo isotopes can be used as an efficient proxy to trace the mantle source heterogeneity,[21] subduction process, crust formation[17,22] and igneous processes.[22–24] Mo is also an essential but scarce micronutrient in biological systems.[25,26] Molybdenum isotopes hold great potential for deciphering Mo's biochemical reactions, displaying a wide range of Mo isotope fractionation concomitant with basic physicochemical processes.[27]

However, since Mo content in volcanic rocks such as the mid-ocean-ridge basalts (MORB), granites (<100 ng g^{-1}),[28] and most plants (0.1–1 μg g^{-1} of dry weight)[29] is relatively lower, determining Mo isotopes in samples with low or ultra-low Mo contents is still challenging, which restricted the further applications of Mo isotopes in studying the biogeochemical

[a]*State Key Laboratory of Geological Processes and Mineral Resources, China University of Geosciences (Beijing), Beijing 100083, China. E-mail: jmzhu@cugb.edu.cn; Tel: +86-010-82322832*

[b]*State Key Laboratory of Environmental Geochemistry, Institute of Geochemistry, Chinese Academy of Sciences, Guiyang, 550081, China*

† Electronic supplementary information (ESI) available. See DOI: 10.1039/d1ja00465d

cycle of Mo in the Earth's surface from the local to the global scale. In order to obtain the highly precise and accurate Mo isotopes for these kinds of samples, large sample sizes up to 1–5 g should be required to separate Mo using the current purification protocol,[30] posing an insurmountable shortcoming for chemical purification and complex matrix elimination.

Several Mo separation schemes have been proposed in previous studies using either a single column of an anion and a cation exchange resin or a two-column combining both.[4,26] Most separation protocols were successfully applied to Mo-rich samples, and a few designed to process low-Mo samples were proposed. For example, by resorting to the double-spike (DS), Willbold *et al.* (2016)[30] developed a new and efficient single-column Mo separation scheme with a low Mo blank to extract Mo from basalts and steel. Simultaneously, Liu *et al.* (2016)[32] presented a method with 0.6 ng of Mo blank, in which the amount of Mo pulled from carbonate rocks was reduced to 100 ng. More recently, Liang *et al.* (2016)[33] reported that the concentration of Mo in all the analyzed solutions had been reduced to 15–30 μg L^{-1}. However, owing to the high procedural blank of ≥1–3 ng, a large sample size, some even up to 1 g, was still needed to separate Mo. In contrast, with the help of extremely low total blanks (30–190 pg), Li *et al.* (2014)[34] and Fan *et al.* (2020)[28] used BPHA (*N*-benzoyl-*N*-phenylhydroxylamine) to extract Mo from low-Mo rock samples (10–500 ng g^{-1}). However, BPHA is commercially unavailable, hindering its widespread application.

In addition, among most of the previous methods, isotope determination at high concentration (>50 ng g^{-1}) makes it challenging to analyze repeatedly, which further impedes high precision $\delta^{98/95}$Mo determination of low Mo geological and environmental samples. Improving the instrumental sensitivity and reducing the sample size for purification and measurement are the best ways to obtain precise Mo isotope composition for extremely low-Mo samples. Malinovsky *et al.* (2018)[27] attempted to measure Mo isotopes at 10–15 ng mL^{-1} level by enhancing the sensitivity (typical ^{98}Mo sensitivity = 100 V μg^{-1} mL^{-1}) using a desolvating Apex – Q sample inlet system with a small amount of EDTA in sample solutions and Natalie *et al.* (2020)[35] enhanced the typical sensitivity of 100–140 V μg^{-1} g^{-1} Mo for ^{96}Mo. But the precision of the measured $\delta^{98/95}$Mo values was poor, with 0.1 to 0.2‰. These precisions could not identify the smaller Mo isotope variations often found in various biogeochemical processes. Therefore, determining Mo isotopes with high sensitivity and precision becomes increasingly crucial in reducing blanks and further reducing sample size for Mo purification.

In order to measure Mo isotopes of low Mo samples with higher precision and accuracy and eliminate complex matrices, reducing sample size and simultaneously improving instrumental sensitivity are better ways to solve the issues above. Here, according to a cleaning scheme proposed to minimize the total blank of less than 0.16 ng involving the commercially available Muromac®1X8 (a kind of AG1-X8) anion and AG50-X8 cation-exchange resin, the samples containing 30–60 ng Mo are ensured sufficient to purify for isotope measurement three more times. Meanwhile, the Mo isotope measurement with high sensitivity (^{95}Mo = 200–330 V μg^{-1} mL^{-1}) was achieved using an improved Aridus II with an ice chamber in the sample introduction system (SIS). The $\delta^{98/95}$Mo values of some recommended geological reference materials (GRMs) analyzed at 5 and 10 ng of Mo levels are remarkably consistent with the published data, yielding an external precision better than 0.06‰ (2SD). These results validate the accurate and precise Mo isotope determinations and the reliability of our analytical method, which is helpful to explore the application of Mo isotopes in investigating the global cycle of Mo in nature and metabolic processes of Mo in plants, animals, and human tissues or organs.

2. Experimental methods

2.1. Chemical reagents and materials

All the used optima-grade hydrochloric acid (HCl), hydrofluoric acid (HF), and nitric acid (HNO_3) (Beijing Institute of Chemical Reagents, China) were further purified once using Savillex™ DST-1500 stills (a sub-boiling acid distillation system). Ultrapure water (18.2 MΩ cm^{-1}) was prepared by the Milli-Q Element system (Millipore, USA). The highly pure chemical reagents, including 35% H_2O_2 (trace metal grade), Specpure® plasma standard solution of Mo with 10 000 μg g^{-1} (in 5% HNO_3/tr. HF, lot. 41-551010A), Zr, Ru, and Pd (1000 μg g^{-1}), were obtained from Alfa Aesar Ltd (Johnson Matthey Company: JMC) in China. Mo standard solution (NIST SRM 3134: lot. 130418) was purchased from the National Institute of Standard and Technology (NIST), USA. Drs Xiang-Kun Zhu and Jin Li provided a different batch number of NIST SRM 3134 (lot. 891307). All the PFA beakers (Savillex™), centrifuge tubes, and pipette tips were strictly cleaned according to the procedures described by Zhu *et al.* (2018).[36] All sample pre-treatments were performed in class 1000 ultra-clean room, and chemical purification was carried out in a class 100 hood at the isotope geochemistry laboratory, China University of Geosciences (Beijing).

2.2. Sample preparation and digestion

A variety of geological and environmental reference materials (RMs) were employed to evaluate the reliability of our improved chemical separation and measurement protocol. Some of them have certified Mo isotope compositions in previous works, allowing intercalibration with results obtained in this study. These international RMs were purchased from the United States Geological Survey (USGS, USA), National Institute of Standard and Technology (NIST, USA), Ocean Scientific International Limited (OSIL, UK), and Institute of Geophysical and Geochemical Research (IGGE, China), including Atlantic seawater (IAPSO), basalt, andesite, granite, carbonate, shale, manganese nodules, cobalt-rich crusts, soils, sediments, loess, plant samples, and animal tissues. The different digestion schemes were employed to decompose various samples with the different characteristics described in detail in Zhu *et al.* (2018).[36] Briefly, the digestion procedures are presented below.

Unlike some studies in which a double spike (DS) was mixed with sample powder before digestion, we first decomposed all

samples into a solution to avoid DS contaminating digestion vessels and waste DS due to widely variable Mo content in different samples.[36,37] Hereby, a set of silicate samples, including basalt, andesite, and granite powders, were carefully weighed ~50 mg into the individual 15 mL PFA beakers. 3 mL of mixed acid (HF (23 M) : HNO_3 (15.8 M) = 2 : 1) was added, followed by repeatedly heating the sealed PFA beakers at 140 °C and sonication (15 min) until no precipitate was observed. The solutions were dried down to incipient dryness and then dissolved in 3 mL of *aqua regia* (HCl : HNO_3 = 3 : 1) for digesting again until the clear solution was obtained in 1 mL of 10% HNO_3 (v/v). For shale, sediment, soil, loess, plant, and animal tissue reference materials, approximately 100 mg samples were decomposed at 185 °C ± 5 °C for 36–48 h in customized high-pressure bombs with 3.0 mL of a mixture of HNO_3 (15.8 M) and HF (23 M). After cooling, 1 mL 35% H_2O_2 and 0.4 mL of HF (23 M) were added, and the samples were evaporated to incipient dryness at 130 °C. They were then further digested with 3 mL of a 10 : 1 mixture of HNO_3 and HF for 16 h at 185 °C ± 5 °C, repeating the above steps until clear solutions were achieved in 1 mL of 10% HNO_3 (v/v). For carbonate, manganese nodules, and Co-rich crusts samples, typically ~100 mg (~200 mg for JDO-1) of sample powders were weighted into 30 mL PTFE liners, and 6 M HCl was added to degas for 2 h. They were then evaporated to near dryness. 3 mL of concentrated HNO_3 was added, and the sealed bombs were placed in a pre-heated oven at 185 ± 5 °C for 24 h. After cooling, the solutions were transferred into 15 mL PFA beakers to evaporate. The residues were dissolved in 1 mL 10% HNO_3 and transferred into 6 mL centrifuge tubes with a small amount of undissolved material for storage. Only the supernatant of these samples was used to purify after centrifuging for 20 min at 3600 rpm.

2.3. Mo purification

Before purification, sample aliquots containing 30–60 ng Mo were mixed with the ^{97}Mo–^{100}Mo double spike (DS) in 15 mL Savillex PFA beakers at the optimized ratio of $^{100}Mo_{spike}/^{98}Mo_{sample}$ = 2.75. To the spiked sample solutions were added ~0.5 mL 15 M HNO_3, and the beakers were tightly screwed up and put on a hot plate overnight at 100 °C for sample-spike equilibration. After that, the beakers were cooled to room temperature and evaporated to dryness at 100 °C. Subsequently, the samples were re-dissolved in 0.6 mL of ~8.8 M HCl solution, and they were then placed on the hotplate at 100 °C for 30 min followed by Mo separation (Table 1).

2.3.1 Column I for removing Ca and Fe. Column I (10 mL of Bio-Rad polypropylene column) pre-loaded with 2 mL of AG50W-X8 cation resin (200–400 m, Bio-Rad) were cleaned strictly according to the procedures listed in Table S1† and washed to near neutral with MQ water, and then conditioned with 3 mL of 10.5 M HCl. 0.6 mL of spiked sample solution was loaded onto the resin followed by 5.5 mL of 10.5 M HCl (6 × 0.91 mL) and ~6.1 mL of Mo was collected during loading and diluted to 8 M HCl–0.1 M HF media by adding 33 μL HF (24 M) and 1.78 mL MQ water for column II.

Table 1 Separation scheme of Mo from geological and environmental samples

Separation stage	Reagent	Volume/ml
Column I *(removing Fe and Ca)*: cation exchange resin (AG50W-X8, 200–400 mesh, 2 mL)		
Condition	10.5 M HCl	3
Load sample and collect Mo	8.80 M HCl	0.6
Collect Mo	10.5 M HCl	5.5
Clean resin	MQ H_2O	10
Column II: anion exchange resin (AG1-X8, 100–200 mesh, 2 mL)		
Condition	8 M HCl + 0.1 M HF	4
Load sample	8 M HCl + 0.1 M HF	7.9
Elute matrix	8 M HCl + 0.1 M HF	4
Elute matrix	6 M HCl + 0.1 M HF	13
Elute matrix	6 M HCl	13
Elute matrix	4 M HCl	6
Elute Fe	0.5 M HCl + 0.1% H_2O_2	14
Elute Fe	1 M HCl + 0.5 M HF	4
Collect Mo	8 M HF + 2 M HCl	12
Clean resin	MQ H_2O	
Column III: cation exchange resin (AG50W-X8, 200–400 mesh, 2 mL)		
Condition	0.5 M HCl + 0.3% H_2O_2	8
Load sample and collect Mo	0.5 M HCl + 0.3% H_2O_2	2
Collect Mo	0.5 M HCl + 0.3% H_2O_2	12
Clean resin	MQ H_2O	10

2.3.2 Columns II for removing Zr, Ni, and Fe. Column II was filled with 2 mL of Muromac®1X8 anion resin (100–200 m, Muromac®, Japan) and preconditioned with 8 M HCl–0.1 M HF. The beakers containing ~8 mL diluted eluent were immediately put on a hotplate at 80 °C for 30 min. After cooling, samples (8 × 1 mL) were loaded, followed by 4 mL of 8 M HCl–0.1 M HF, 13 mL 6 M HCl–0.1 M HF, and 13 mL 6 M HCl rinsing to eliminate Zr, Ru, Cu, Ni, and most matrix elements. Subsequently, the resin was washed by adding 6 mL 4 M HCl, 14 mL 0.5 M HCl–0.1% H_2O_2, and 1 M HCl–0.5 M HF to clear up Fe and other small amounts of matrix elements. Finally, Mo was eluted using 8 M HF–2 M HCl (12 × 1 mL) and collected in clean PFA beakers.

2.3.3 Column III for obtaining high-purity Mo. Column III was used to remove possible residual matrix elements such as tiny amounts of Fe and Zn.[38] The dried samples from column II were dissolved in 1 mL 0.5 M HCl, then 6 μL H_2O_2 and 1 mL 0.5 M HCl were added to make a solution of 2 mL 0.5 M HCl–0.3% H_2O_2. The solutions were loaded onto column III that pre-filled 2 mL of AG50W-X8 cation resin (200–400 m, Bio-Rad) and conditioned with 8 mL 0.5 M HCl + 0.3% H_2O_2. Column III was rinsed with 12 mL 0.5 M HCl + 0.3% H_2O_2 (v/v). All eluents (14 mL) were collected in 15 mL PFA beakers and dried down. Finally, purified Mo was dissolved in 2% HNO_3–0.1% HF (v/v) for mass spectrometry.

2.4 Mo isotopes measurement

2.4.1. Mo double spike. As in previous studies, the ^{97}Mo–^{100}Mo double spike was also utilized in our work to correct for isotope fractionation from instrumental mass bias

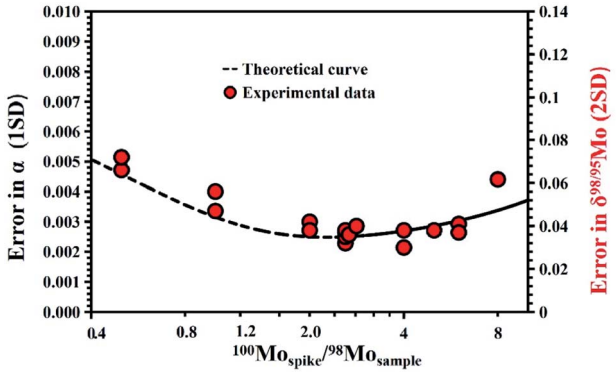

Fig. 1 The best mixing ratio of the spike ($^{100}Mo_{spike}$) to sample ($^{98}Mo_{sample}$) by theoretical simulation (dotted curve) and experimental measurement (red circles) at $^{97}Mo_{spike}/^{100}Mo_{spike} = 1$. The left and right *y*-axes show the variation of the theoretical error in α (fractionation factor of natural samples relative to SRM 3134) and the measured error in $\delta^{98/95}$Mo, respectively.

and chemical purification. Single spikes of ^{97}Mo (96.60%) and ^{100}Mo (99.03%) were bought from ISOFLEX (USA) and separately dissolved in 7 M HNO_3 with a little HCl. The aimed double spike composition was calibrated to be $^{97}Mo : {}^{100}Mo = 1.009200$ using NIST 3134 (lot. 130418) by a standard-sample-bracketing (SSB) method on Nu Plasma II MC-ICP-MS (Nu II). This ratio is very close to the result provided by Siebert *et al.* (2001).[39] To accurately measure Mo isotopes with minimizing error propagation, the optimized mixing range of $^{100}Mo_{spike}/^{98}Mo_{sample}$ was acquired to be 1.5 to 8 through a Monte Carlo – nest iteration program, and the best ratio of $^{100}Mo_{spike}/^{98}Mo_{sample}$ was 2.75 (Fig. 1). This observation can be found in detail in the literature.[40–42] Consequently, a $^{100}Mo_{spike}/^{98}Mo_{sample}$ ratio of 2.75 was employed for all samples and standard solutions. For actual samples, the ratio of $^{100}Mo_{spike}/^{98}Mo_{sample}$ was sometimes less than or greater than 2.75 due to the incorrect Mo concentrations. Still, the precision and accuracy of $\delta^{98/95}$Mo would not be affected as long as the $^{100}Mo_{spike}/^{98}Mo_{sample}$ ratio ranges from 1.5 to 8.

2.4.2. Mass spectrometry. Molybdenum isotope measurements were mainly performed on a Neptune Plus MC-ICP-MS (NP) at the Laboratory of Isotope Geochemistry, China University of Geosciences (Beijing). Double spike calibration was conducted on a Nu II at the State Key Laboratory of Environment Geochemistry, Institute of Geochemistry, Chinese Academy of Sciences. As shown in Table 2, eight Faraday cups monitor the signals of Mo isotopes and ^{91}Zr at a low resolution on NP. $^{97}Mo^+$ and $^{99}Ru^+$ were simultaneously measured on C and H2 cup in sub-configure for getting the ratio of ^{97}Mo/^{99}Ru to subtract ^{96}Ru, ^{98}Ru, and ^{100}Ru isobaric interference onto ^{96}Mo, ^{98}Mo, and ^{100}Mo. Similarly, eleven Faraday cups were employed on Nu II at the static mode and low resolution. $^{56}Fe^{40}Ar^+$ was also monitored *via* $^{57}Fe^+$ using Ax cup without changing Quads setting for Mo isotopes. Signals were collected for 3 blocks, each with 15 cycles and each cycle with 4.194 s integration time for NP; while 3 blocks of 10 cycles with 10 s integration time for each one were used on Nu II. The on-peak blank was determined before in 2% HNO_3–0.1% HF (v/v) and then subtracted from the subsequent sample signals on both instruments.

Purified samples dissolved in 2% HNO_3–0.1% HF were introduced into the plasma by an Aridus II desolvator (Cetac Technologies Omaha, NE, USA) sample introducing system (SIS) installed with an ESI Teflon aspire nebulizer (100 μL mL^{-1}) *via* a Cetac AXR112 autosampler. The ^{95}Mo signal intensity was 2.0–3.3 V on the NP at the Mo concentration of 10 ng mL^{-1} while 2.0–3.5 V on the Nu II at 100 ng mL^{-1}. Thereby, sample solutions with 10 ng mL^{-1} (10 ng = 110 μL min^{-1} × 9 min × 10

Table 2 Neptune Plus and Nu Plasma II MC-ICP-MS operating parameters for Mo isotope measurements

Parameters	Settings for NP	Settings for Nu II
Cup configuration	L4(^{91}Zr), L3(^{92}Mo), L2(^{94}Mo) L1(^{95}Mo), C(^{96}Mo), H1(^{97}Mo) H2(^{98}Mo), H3(^{100}Mo) Sub config. C(^{97}Mo), H2(^{99}Ru)	L5(^{90}Zr), L4(^{92}Mo), L2(^{94}Mo), L1(^{95}Mo), Ax(^{96}Mo) H1(^{97}Mo), H2(^{98}Mo), H3(^{99}Ru), H4(^{100}Mo) H6(^{102}Ru,^{102}Pd), H7(^{104}Pd)
RF power	1250 W	1300 W
Sampler cone (nickel)	H Cone	541B (1.15 mm)/dry cone (0.9 mm)
Skimmer cone (nickel)	X cone	540 (0.6 mm orifice)/dry cone
Cooling Ar_2 flow rate	15 L min^{-1}	13 L min^{-1}
Auxiliary Ar_2 flow rate	0.8 L min^{-1}	0.8 L min^{-1}
Nebulizer Ar_2 flow rate	0.90–1.05 L min^{-1}	25–33 psi
Cycle integration time	4.194 s	10 s
Number of cycles	45	30
Sensitivity of ^{95}Mo	200–330 V ppm^{-1}	15–20 V ppm^{-1}
Aridus II		
Sweep gas flow rate	3.5–4.8 L min^{-1}	3.0–3.9 L min^{-1}
Nitrogen (N_2) flow rate	0.02–0.05 L min^{-1}	No
T of spray chamber[a]	110 °C	110 °C
T of desolator	160 °C	160 °C
Sample uptake rate	110 μL min^{-1}	100 μL min^{-1}

[a] *T* represents temperature.

μg L^{-1}) for NP and 100 ng mL^{-1} for Nu II were generally employed for measuring Mo isotopes. Spiked NIST 3134 solution was analyzed every 3–5 samples to monitor the instrument stability and normalize the sample data.

Since NIST 3134 has been recommended as an international standard for Mo isotopes,[32,43,44] all isotopic data are reported as the delta notation relative to NIST 3134 (lot. 130418): $\delta^{98/95}Mo = [(^{98}Mo/^{95}Mo)_{sample}/(^{98}Mo/^{95}Mo)_{3134} - 1] \times 1000‰$. $\delta^{98/95}Mo$ and $\delta^{96/95}Mo$ were reduced *via* an offline EXCEL worksheet on the NP while an online DS program, similar to Cd isotope data reduction,[36,37] was built into the executive program to extract ratios on the Nu II. Since JMC Mo solution was used as Mo isotope standard in previous studies, the conversion between $\delta^{98/95}Mo_{NIST3134}$ and $\delta^{98/95}Mo_{JMCMo}$ was conducted to facilitate inter-laboratory comparison in terms of $\delta^{98/95}Mo_{JMC} = \delta^{98/95}Mo_{NIST3134} + \delta^{98/95}Mo_{NIST3134\text{-}JMC} + (\delta^{98/95}Mo_{NIST3134} \times {}^{98/95}Mo_{NIST3134\text{-}JMC}) \times 10^{-3}$. Here, $^{98/95}Mo_{NIST3134\text{-}JMC}$ is equal to 0.25‰, as suggested by Nägler *et al.* (2014).[45]

3. Results and discussion

3.1. Separation scheme of Mo

Previous studies have proposed several Mo separation schemes for different types of geological and environmental samples. Most of them separated Mo from sample matrices either by a single AG® MP-1M/AG1-X8 anion resin or by combining cation (AG50W-X8 or Dowex™ 50W-X8) and anion (AG1-X8 or Dowex™ 1-X8) resins. Since Mo likely contaminated the AG® MP-1M resin we bought from Bio-Rad and caused the highly procedural blank, we chose Muromac®1X8 instead of AG® MP-1M anion resin for our improved Mo separation scheme with consistently >90% yields for various samples. This purification scheme (Table 1), mainly consisting of the cation and anion exchange resins, was modified from previous protocols.[30,36,41,46]

As demonstrated by Zhu *et al.* (2018),[36] column I can effectively remove most Ca (>90%) and Fe (>80%) while other elements including Mo, Ti, Cr, Co, Ni, Cu, and Zn are still in the eluent. Since Mo(VI) exists as the predominant form of complex $MoOCl_5^-$ in ≥7 M HCl whereas MoO_2^{2+} and MoO^{4+} in ≤1 M HCl, 7 M HCl was employed to extract Mo from sample matrices through AG® MP-1M resin[41] while 1 M HCl was utilized to elute Mo in AG1-X8 resin.[30,32] Thus, the eluents with 10.5 M HCl from column I were diluted to be 8 M HCl–0.1 M HF and then loaded onto column II to hold Mo, followed by rinsing with 8 M HCl–0.1 M HF, 6 M HCl–0.1 M HF, and 6 M HCl to remove most matrix elements such as Zr, W, Cr, Co, Ni, Cu, *etc.* However, low-Mo samples (<0.5 μg g^{-1}) generally have a high ratio of [Fe]/[Mo] more than 30 000 (Table 3), and Fe should be further eliminated. Previous studies have shown that 4 M HCl can effectively elute Fe, but when ≥8 mL of 4 M HCl was used to rinse column II after 6 M HCl, a little bit of Mo will be lost in our experiment. Willbold *et al.* (2016)[30] and Li *et al.* (2016)[46] utilized 0.5 M HCl–0.3% H_2O_2 and 1 M HCl–0.5 M HF to elute some matrix elements and Fe in AG1-X8 resin while Mo was still retained.[30,46] Therefore, modifications were made to our purification procedures using 6 mL 4 M HCl, 14 mL 0.5 M HCl + 0.1% H_2O_2 and 4 mL 1 M HCl + 0.5 M HF to avoid the loss of Mo. After this, Mo fraction was collected in 12 mL of 8 M HCl–0.1 M HF. Because Mo isotopes were determined at the high-sensitivity model, a tiny amount of Fe at [Fe]/[Mo] ≥ 0.5 will produce $^{54}Fe^{40}Ar^+$, $^{56}Fe^{40}Ar^+$ and $^{57}Fe^{40}Ar^+$ in plasma, forming the interference on $^{94}Mo^+$, $^{96}Mo^+$ and $^{97}Mo^+$. Consequently, as suggested by Voegelin *et al.* (2009)[47] that 0.5 M HCl + 0.3% H_2O_2 can separate Mo effectively, column III was still utilized for 2 mL of AG50W-X8 cation resin to hold a tiny amount of residual Fe and Zn, and Mo was eluted immediately and collected. The distinguishing features of this purification scheme are its high efficiency, flexibility, and wide applicability to various geological samples.

3.2 Sensitivity of determining Mo isotopes and data validation

In order to enhance the measurement sensitivity and eliminate spectral interferences, nitrogen (N_2) and the improved Aridus II with ice chamber in the SIS were set up.[37,48] The addition of trace N_2 on NP not only suppresses the interferences (*e.g.*, $^{40}Ar^{40}Ar^{16}O^+$) but also improves sensitivity. The improved Aridus II with an ice chamber can increase the transmission efficiency of the analyte and maintain good stability during the analytical session.[48] Thus, the sensitivity of ^{95}Mo signal (generally ~200 V ppm^{-1} for ^{95}Mo, the maximum is ~330 V ppm^{-1} depended on the different NP and its equipped eroded slit size) on NP is much higher than that previously reported using desolvating Apex – Q sample inlet system (Table 2).[27] This indicates that ^{95}Mo signal can achieve ~1.0 V for a 5 ng mL^{-1} injecting solution.

Nevertheless, such a higher sensitivity can easily cause unwanted side effects such as stronger memories. To eliminate the memory effects of Mo in SIS, the N_2 should be adjusted slightly to suppress the baseline. Simultaneously, Aridus II is kept rising by 2% HNO_3–0.1% HF for at least eight minutes until the ^{95}Mo signal is less than 1 mV, and on-peak zero (OPZ) is conducted to spiked samples and standard solution. Through those ways, the sensitivity and stability of signals can be significantly improved while memory and interference are obviously reduced.

To evaluate the data validity, the RMs, SDO-1, SRG-1b, BCR-2, COQ-1, and NOD-P-1 were determined repeatedly at Mo concentrations of 5, 10, ≥20 ng mL^{-1} (Fig. 2). The average $\delta^{98/95}Mo$ and 2 standard deviation ($n = 3$) of SDO-1, SRG-1b, BCR-2, COQ-1, and NOD-P-1 are 0.83 ± 0.05‰, 0.43 ± 0.04‰, −0.04 ± 0.03‰, −0.20 ± 0.02‰, and −0.86 ± 0.04‰ at 5 ng mL^{-1}; 0.82 ± 0.04‰, 0.43 ± 0.04‰, −0.03 ± 0.02‰, −0.21 ± 0.02‰, and −0.86 ± 0.03‰ at 10 ng mL^{-1}, and 0.81 ± 0.03‰, 0.42 ± 0.03‰, −0.03 ± 0.03‰, −0.19 ± 0.03‰, −0.87 ± 0.03‰ at ≥20 ng mL^{-1}, respectively. These values are greatly consistent with the published results. There is no significant difference among them, demonstrating that high-precision (2SD ≤ 0.05‰) Mo isotopes can be obtained at 5 and 10 ng Mo levels, even at 3 ng.

3.3. Evaluation of isobaric interference

The major potential interferences in determining Mo isotopes are spectral interferences, mainly doubly charged ions, polyatomic and isobaric ions.[44] Under the high-sensitivity setup,

Table 3 Mo concentration and isotope composition of geological and environmental reference materials

Sample name	Sample type	Reference	Mo (μg g^{-1})	Fe/Mo	$\delta^{98/95}Mo_{3134}$	2SD	N[b]	Fe/Mo after purification	$\delta^{98/95}Mo_{JMC}$
BCR-2	Basalt	This study	256	556	−0.03	0.04	6	<0.01	0.22[a]
		Li *et al.* (2016)[46]	329		−0.04[a]	0.07	3	—[d]	0.21
		Skierszkan *et al.* (2015)[41]	—		−0.04	0.1	—	—	0.21[a]
		Liu *et al.* (2016)[32]	**—**		**0.22**[a]	**0.09**	**12**	**—**	**0.47**
		Liang *et al.* (2016)[33]	236		−0.03	0.04	—	—	0.22[a]
BHVO-2	Basalt	This study	3.3	36 176	−0.03	0.05	8	<0.01	0.22[a]
		Burkhardt *et al.* (2014)[23]	4.55		−0.06	0.03	23	—	0.19[a]
		Willbold *et al.* (2016)[30]	4.2		−0.07	0.04[c]	48	—	0.18[a]
		Yang *et al.* (2015)[16]	3.5		0.01	—	—	—	0.26[a]
		Zhao *et al.* (2016)[49]	3.38		−0.05	0.09	5	—	0.20[a]
		Migeon *et al.* (2015)[64]	4.4		−0.04	0.02[c]	—	—	0.21[a]
		König *et al.* (2016)[17]	3.5		−0.07	0.03	6	—	0.18[a]
		Liang *et al.* (2016)[33]	3.48		−0.03	0.04	—	—	0.22[a]
		Feng *et al.* (2020)[51]	—		−0.03	0.05	12	—	0.22[a]
GSR-3		This study	2.81	51 538	−0.53	0.06	5	<0.01	−0.28[a]
		Zhao *et al.* (2016)[49]	2.92		−0.51	0.04		—	−0.26[a]
GSR-2	Andesite	This study	0.51	90 741	−0.14	0.01	4	<0.01	0.11[a]
		Zhao *et al.* (2016)[49]	0.58		−0.28	0.07	5	—	−0.03[a]
AGV-2		This study	1.72	34 308	−0.15	0.02	4	<0.01	0.10[a]
		Willbold *et al.* (2016)[30]	1.96		−0.15	0.01[c]	3	—	0.10[a]
		Zhao *et al.* (2016)[49]	1.95		−0.14	0.05	5	—	0.11[a]
		Feng *et al.* (2020)[51]	—	—	−0.12	0.08	7	—	0.13[a]
GSR-1	Granodiorite	This study	3.5	16 355	0.094	0.01	3	<0.01	0.34[a]
GSP-2		This study	2.08	23 333	−0.21	0.01	3	<0.01	0.04[a]
		Yang *et al.* (2015)[16]	2.1		−0.17				0.08[a]
JDO-1	Dolomite	This study	0.22	945	0.50	0.02	3	<0.01	0.75[a]
GSR-6	Limestone	This study	0.35	406	0.30	0.02	6	<0.01	0.55[a]
		Liu *et al.* (2016)[32]	**—**		**0.51**[a]	**0.09**	**12**	**—**	**0.76**
COQ-1	Carbonatite	This study	6.8	3973	−0.20	0.02	3	<0.01	0.05[a]
		Zhao *et al.* (2016)[49]	7.4		−0.26	0.10	5	—	−0.01[a]
SGR-1b	Shale	This study	32.5	572	0.42	0.03	4	<0.01	0.67[a]
		Li *et al.* (2016)[46]	44.7		0.38[a]	0.02	3	—	0.63
		Zhao *et al.* (2016)[49]	35.5		0.44	0.11	5	—	0.69[a]
SDO-1		This study	133	697	0.82	0.05	4	<0.01	1.07[a]
		Asael *et al.* (2013)[50]			0.74	0.08			0.99[a]
		Goldberg *et al.* (2013)[44]	—		0.80	0.12	—	—	1.05[a]
		Skierszkan *et al.* (2015)[41]	—		0.79	0.05	—	—	1.04[a]
SCO-1		This study	1.11	37 518	−0.44	0.04	4	<0.01	−0.19[a]
		Li *et al.* (2016)[46]	1.4		−0.49[a]	0.06	5	—	−0.24
		Zhao *et al.* (2016)[49]	1.2		−0.41	0.03	5	—	−0.16[a]
GSMC-1	Cobalt-rich crusts	This study	480	404	−0.97	0.05	4	<0.01	−0.72[a]
		Zhao *et al.* (2016)[49]	466		−0.94	0.07	5	—	−0.69[a]
GSMC-2		This study	520	544	−0.94	0.05	4	<0.01	−0.69[a]
CSMC-3		This study	435	400	−0.96	0.05	4	<0.01	−0.71[a]
NOD-A-1	Manganese nodule	This study	448	348	−0.65	0.02	4	<0.01	−0.40[a]
		Barling *et al.* (2001)[7]	—		−1.21[a]	0.15	—	—	−0.96
		Asael *et al.* (2013)[50]	—		−0.68	0.04	10	—	−0.43[a]
		Li *et al.* (2016)[46]	483.5		−0.73	0.05	6	—	−0.48[a]
		Zhao *et al.* (2016)[49]	589		−0.83	0.05	5	—	−0.58[a]
		Feng *et al.* (2020)[51]			−0.70	0.05	5	—	−0.45[a]
NOD-P-1		This study	760	109	−0.86	0.03	15	<0.01	−0.61[a]
		Barling *et al.* (2001)[7]	—		−0.89[a]	0.15	—	—	−0.64
		Asael *et al.* (2013)[50]	—		−0.83	0.10	5	—	−0.67[a]
		Li *et al.* (2016)[46]	776.5		−0.91[a]	0.05	3	—	−0.66[a]
		Zhao *et al.* (2016)[49]	637		−0.88	0.01	5	—	−0.63[a]
		Feng *et al.* (2020)[51]			−0.86	0.03	5	—	−0.61[a]
CLB-1	Coal	This study	10.3	1389	1.25	0.03	4	<0.01	1.50[a]
GSS-5	Soil	This study	4.38	27 435	0.26	0.01	3	<0.01	0.51[a]
GSS-6		This study	0.45	4494	0.43	0.04	3	<0.01	0.68[a]
GSS-12		This study	1.01	49 063	−0.31	0.03	3	<0.01	−0.06[a]
GSS-14		This study	0.61	81 846	−0.34	0.03	3	<0.01	−0.09[a]
GSS-16		This study	1.01	47 304	−0.29	0.01	3	<0.01	−0.04[a]

Table 3 (*Contd.*)

Sample name	Sample type	Reference	Mo (μg g^{-1})	Fe/Mo	$\delta^{98/95}Mo_{3134}$	2SD	N[b]	Fe/Mo after purification	$\delta^{98/95}Mo_{JMC}$
GSS-20		This study	3.05	12 875	0.32	0.03	3	<0.01	0.57[a]
2711a		This study	1.64	16 207	−0.08	0.01	3	<0.01	0.17[a]
GSS-8	Loess	This study	1.08	38 621	−0.16	0.03	3	<0.01	0.09[a]
GSS-24	Beach sediment	This study	1.05	45 182	0.09	0.04	3	<0.01	0.34[a]
GSS-27	Changjiang sediment	This study	0.94	72 857	−0.02	0.02	3	<0.01	0.23[a]
GSS-28	Xiangjiang sediment	This study	1.11	55 085	−0.23	0.03	3	<0.01	0.02[a]
GBW07319	Tibet sediment	This study	14.3	6671	0.46	0.01	3	<0.01	0.71[a]
GBW07325		This study	5.71	4652	−0.07	0.03	3	<0.01	0.18[a]
GBW07327		This study	5.32	5871	−0.21	0.04	3	<0.01	0.04[a]
GBW07343	Huanghe sediment	This study	0.55	66 825	0.09	0.02	3	<0.01	0.34[a]
GBW07345		This study	0.52	41 129	0.024	0.01	3	<0.01	0.27[a]
GSD-3	Steam sediment	This study	75.7	711	−0.48	0.02	3	<0.01	−0.23[a]
GSD-5		This study	1.58	48 667	−0.39	0.03	3	<0.01	−0.14[a]
GSD-7a		This study	0.76	50 976	−0.35	0.01	3	<0.01	−0.10[a]
GSD-12		This study	7.30	5810	−0.19	0.03	3	<0.01	0.06[a]
GSD-15		This study	0.81	74 468	0.41	0.03	4	<0.01	0.66[a]
GSD-17		This study	3.01	23 750	−0.16	0.05	3	<0.01	0.09[a]
GSD-19		This study	1.04	75 119	−0.042	0.02	3	<0.01	0.21[a]
GSD-21		This study	1.95	28 235	0.40	0.03	3	<0.01	0.65[a]
GSD-22		This study	1.02	34 636	0.13	0.03	3	<0.01	0.38[a]
GSD-23		This study	1.51	45 192	−0.003	0.02	3	<0.01	0.25[a]
GSB-6	Spinach	This study	0.47	1019	0.64	0.03	3	<0.01	0.89[a]
GSB-12	Long bean	This study	4.39	67	0.59	0.04	3	<0.01	0.84[a]
GSB-14	Nori	This study	0.68	0.19	1.47	0.04	3	<0.01	1.72[a]
GSB-19	Astragalus membranaceus	This study	4.82	0.02	0.68	0.05	3	<0.01	0.93[a]
GSB-23	Hunan rice	This study	0.87	7	0.79	0.02	3	<0.01	1.04[a]
GSB-26	Celery	This study	1.07	585	0.78	0.06	3	<0.01	1.03[a]
GSV-1	Shrub leaf	This study	0.37	3923	0.23	0.05	4	<0.01	0.48[a]
GSV-2	Shrub leaf	This study	0.28	3821	0.47	0.02	4	<0.01	0.72[a]
GSB-29	Swine liver	This study	3.98	124	0.42	0.03	4	<0.01	0.67[a]

[a] $\delta^{98/95}Mo_{JMC}$ represents the normalized values by $\delta^{98/95}Mo_{sample\text{-}JMC} = \delta^{98/95}Mo_{sample\text{-}NIST\ SRM\ 3134} + \delta^{98/95}Mo_{NIST\ SRM\ 3134\text{-}JMC} + (\delta^{98/95}Mo_{sample\text{-}NIST\ SRM\ 3134} \times \delta^{98/95}Mo_{JMC\text{-}NIST\ SRM\ 3134}) \times 10^{-3}$, and $\delta^{98/95}Mo_{JMC} = \delta^{98/95}Mo_{SRM\ 3134} + 0.25‰$. [b] The number of repeat measurements for a sample. [c] 2 SE corresponds to the standard error of the mean. [d] —: no data available.

double-charged ions such as $^{184}W^{++}$ and $^{194}Pt^{++}$ were undetectable due to effectively eliminating W and Pt during separation. Isobaric interferences of $^{100}Ru^{+}$ on $^{100}Mo^{+}$ and other Ru isotopes were negligible because of their extremely low concentrations in most samples and were further removed during purification. The elements such as Zr, Cu, Ni, Cr, *etc.*, can also be decreased to insignificant concentration levels using our improved purification procedures.[30,46] Consequently, a tiny amount of residual Fe, Zn, Sn, and occasional Zr in purified solutions may be prone to producing some interferences for the Mo isotope analysis.

To quantify the interference effect of elements aforementioned, we doped the spiked Mo standard solution (NIST 3134) with different proportions of Zr, Fe, Zn, and Sn on the high-sensitivity mode on NP. Fig. 3 shows the $\delta^{98/95}$Mo values corrected by DS do not exhibit the clear deviation when the ratios of [Zr]/[Mo], [Fe]/[Mo], [Zn]/[Mo], and [Sn]/[Mo] are ≤5. However, $\delta^{96/95}$Mo values present the obvious shift at [Zr]/[Mo] ≥ 0.1. Zr isotopes overlap with ^{92}Mo, ^{94}Mo and ^{96}Mo, but do not affect ^{98}Mo. Polyatomic argide ions $^{56}Fe^{40}Ar^{+}$ has also a clear interference on $^{96}Mo^{+}$ at [Fe]/[Mo] ≥ 0.5 while $^{58}Fe^{40}Ar^{+}$ is negligible to $^{98}Mo^{+}$. Nitrogen monoxide ions $^{66}Zn^{14}N^{16}O^{+}$ and $^{68}Zn^{14}N^{16}O^{+}$ and residual matrix element Sn on ^{98}Mo can also be neglected at [Zn]/[Mo] and [Sn]/[Mo] ≤ 5. Thus, for our samples with the initial [Fe]/[Mo] ratio as high as 80 000, they can be reduced to <0.01 after purification using our improved separation procedures, confirming that our improved separation protocol is suitable for various geological and environmental samples, even for ultralow-Mo samples with complex matrices.

3.4 Blanks, precision, and accuracy for Mo isotope analysis

3.4.1 Blank contribution. Reducing the total procedural blank of Mo is a critical prerequisite for sample purification and accurate isotope determination using the sample size only containing ≤30–60 ng Mo. In previous studies, the blank was mainly between 0.2–3 ng except for the specific resin (BHPA: 0.03–0.19 ng) used by Fan *et al.* (2020).[28] The major contributors of the blank were thought to be either H_2O_2, HF, or anion exchange resin.[30] In our experiments, the blank of H_2O_2, HF, and HCl is all less than 0.04 ng and negligible. However, the AG® MP-1M and Ag1-X8 anion resins (Bio-Rad) have higher Mo blank, especially some batches that seem to be contaminated by Mo. Mo concentration in washed eluent from AG® MP-1M

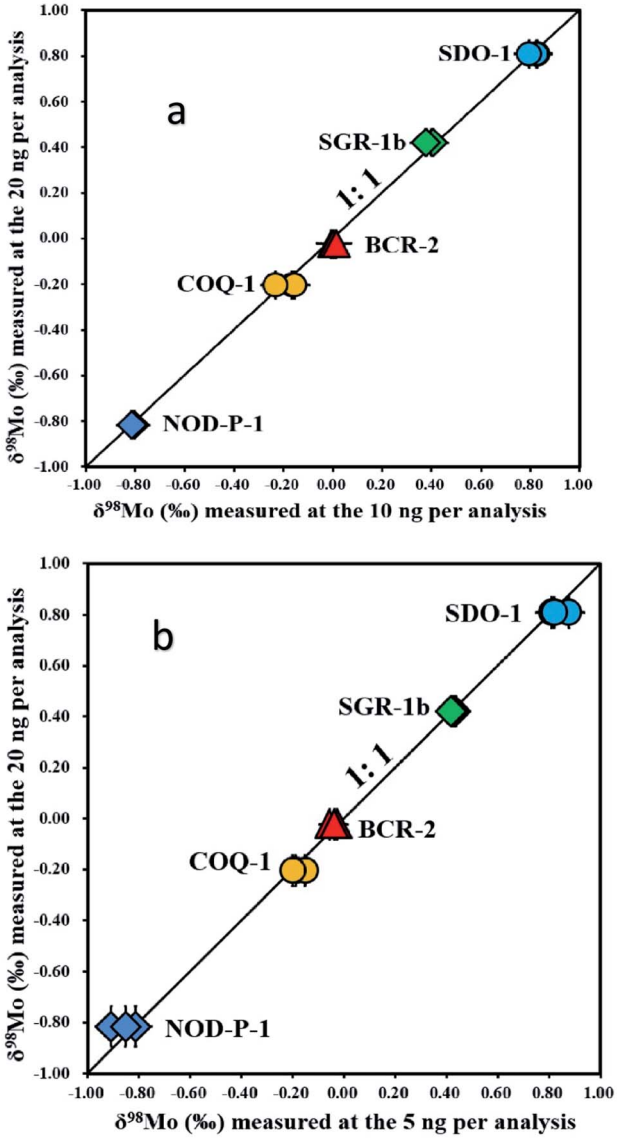

Fig. 2 (a and b) Comparisons of measured results for several GRMs at 5, 10, and 20 ng levels ((a) 10 and 20 ng; (b) 5 and 10 ng).

reaches up to 300 ng mL^{-1}, and its $\delta^{98/95}$Mo is 0.46 ± 0.08‰ (n = 3), implying that the Mo isotope ratio of actual samples is to be either high or low (*e.g.*, seawater) if the blank cannot be eliminated effectively. Thus, an alternative Muromac®1X8 resin was employed in our experiments, and the cleaning procedure is developed and listed in Table S1.†

Using our new cleaning protocol, Mo blank from the resins can be decreased to <0.3 ng after washing three times with 10 mL 3.5 M HNO_3, 20 mL 1 M HCl, 10 mL 0.1 M HCl, and 10 mL 8 M HF + 2 M HCl. Thus, the total blank from the sample digestion to the end of the purification is generally less than 0.16 ± 0.06 ng (n = 10), occasionally 0.45 ± 0.16 ng (n = 5) for the first new resin used. However, to remove the blank effect thoroughly, the cleaner Muromac®1X8 anion resin was prepared and used in all our experiments. Spiked 60 ng NIST 3134, ~60 ng (6 mL), 30 ng (3 mL), and 20 ng (2 mL) IAPSO were processed to evaluate the blank effect. The obtained δ^{98}Mo values of SRM 3134 are consistent with the unprocessed NIST 3134. The average $\delta^{98/95}$Mo value is 2.07 ± 0.04‰ (n = 15) for IAPSO, also identical to the certificated values.[31,34,46,49] These results demonstrate that the blank effect on our purified samples containing ~30 ng Mo is negligible. Additionally, approximately 0.1 ng or a much lower Mo blank can be achieved after using the cleaned resin several times. Therefore, the Muromac®1X8 resin is always used repeatedly in our experiments.

3.4.2 Precision and accuracy. Since our used Mo standard solution (NIST 3134, lot. 130418) is a different batch from that (lot. 891307) certificated by Goldberg *et al.* (2013),[44] long-term measurement was conducted to verify if there was a difference in Mo isotope composition. The $\delta^{98/95}$Mo analyzed on both instruments were 0.00 ± 0.06‰ (n = 352) for lot. 130418 and 0.00 ± 0.06‰ (n = 32) for lot. 891307 relative to lot. 130418 (Fig. 4) over the past three years, showing no resolvable difference between them. As a result, both solutions are homogeneous with the same Mo isotopes, and any of them can be used as a Mo isotope standard solution.

Mo isotope measurement's long-term precision and accuracy were estimated by pure standard solution and geological reference materials (GRMs), including the multiple digested IAPSO, NOD-P-1, SCO-1, SDO-1 AGV-2, BCR-2, and BHVO-2. As shown in Fig. 4 and Table 3, the external precision of pure NIST 3134 (lot. 130418 and lot. 891307), processed NIST 3134 (lot. 130418), and unprocessed JMC-Mo determined on the NP at 10 or 25 ng mL^{-1} were ≤0.05‰ (2SD). The average $\delta^{98/95}$Mo value and 2SD of IAPSO are 2.06 ± 0.05‰ (n = 5), identical with 2.09 ± 0.10‰, 2.04 ± 0.07‰ and 2.13 ± 0.04‰ reported by Goldberg *et al.* (2013),[44] Zhao *et al.* (2016)[49] and Skierszkan *et al.* (2015),[41] respectively. NOD-P-1 is −0.87 ± 0.02‰, greatly consistent with that of −0.89‰, −0.91‰, −0.88‰, −0.83‰ and −0.86‰.[7,46,49–51] The SDO-1 and SCO-1 have been widely used for inter-laboratory calibration. The $\delta^{98/95}$Mo values are 0.82 ± 0.05‰ (n = 4) for SDO-1 and −0.44 ± 0.04‰ (n = 3) for SCO-1, also in excellent agreement with those values 0.80 ± 0.14 (n = 5) and 0.79 ± 0.05 (n = 11) reported by Goldberg *et al.* (2013)[44] and Skierszkan *et al.* (2015),[41] and −0.41 ± 0.05‰ (n = 11) and −0.49 ± 0.05‰ (n = 11) published by Zhao *et al.* (2016)[49] and Li *et al.* (2016),[46] respectively. These results demonstrate that long-term $\delta^{98/95}$Mo precision for natural samples is typically ≤ ±0.05‰ (2SD) for the Neptune Plus MC-ICP-MS.

The results of repeatedly digested AGV-2, BCR-2, and BHVO-2 show a relatively homogeneous Mo isotope composition with a mean $\delta^{98/95}$Mo of −0.15 ± 0.05‰ (n = 6), −0.03 ± 0.04‰ (n = 6), and −0.03 ± 0.05‰ (n = 8), respectively, greatly consistent with the published values (Table 3). BCR-2 and BHVO-2 were thought to be contaminated during rock grinding.[30,46] The detailed discussion on $\delta^{98/95}$Mo in BHVO-2 by Willbold *et al.* (2016)[30] has shown $\delta^{98/95}$Mo values had a narrow variation within uncertainty. Similarly, the Mo isotope compositions of different batches of BCR-2 are within the range of −0.04‰ to 0.01‰ in our study. If they were converted to $\delta^{98/95}Mo_{JMC\text{-}Mo}$ (Table 3), they should be within the scope of 0.21–0.26‰. In comparison with the values (standard-sample bracketing method, 0.39‰ ± 0.04‰ (n = 4) and 0.47‰ ± 0.09‰ (DS, n = 12)) reported by Liu *et al.* (2016),[32] the

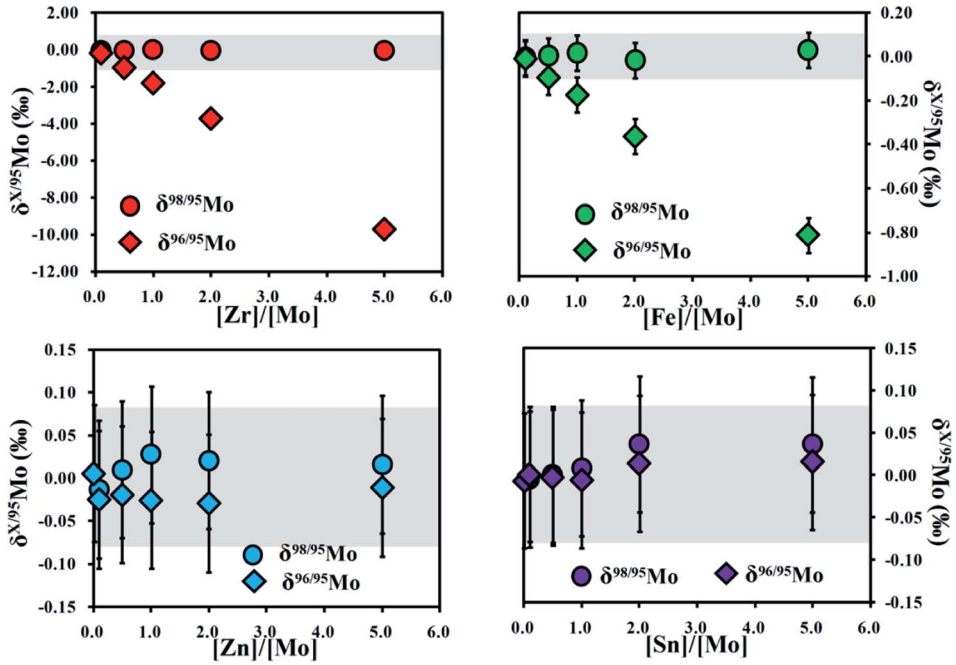

Fig. 3 The effects of different elements with varying [X]/[Mo] on the $\delta^{98/95}$Mo and $\delta^{98/96}$Mo values determined at 10 ng mL^{-1} for NIST 3134. X represents elements and the gray band shows the long-term precision (±0.06‰) on Neptune Plus MC-ICP-MS.

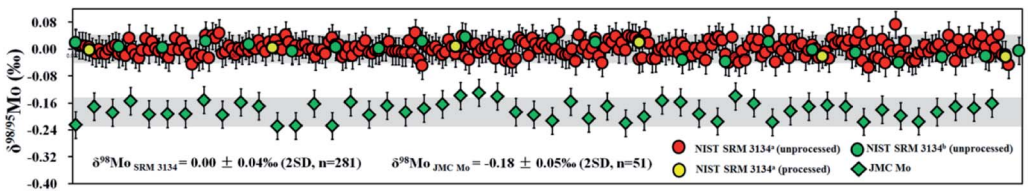

Fig. 4 The long-term reproducibility of $\delta^{98/95}$Mo measured at 10 and 20 ng mL^{-1} on the NP (2SD: ±0.05‰) and 50 or 100 ng mL^{-1} on the Nu II (2SD: ±0.07‰) for NIST 3134 over one year. Error bars represent 2 standard deviations of each measurement. The yellow and green circles represent processed and unprocessed NIST 3134 (lot. 891307: 0.00 ± 0.04‰; 2SD, $n = 28$). The blue triangles denote $\delta^{98/95}$Mo values of JMC Mo standard solution (−0.18 ± 0.05‰; 2SD, $n = 51$).

discrepancy with at least 0.18‰ occurs between the two groups. They explained this observation was due to heterogeneous BCR-2. However, as Willbold *et al.* (2016)[30] demonstrated for BHVO-2, the variations of Mo content in BCR-2 do not mean that their Mo isotopes were heterogeneous. According to the Mo content (248–329 μg g^{-1}) reported by Liu *et al.* (2016)[32] and Li *et al.* (2016),[46] it was almost 50–80 times greater than that in BHVO-2, implying that at least 98% of Mo was from the Mo pollution. Moreover, $\delta^{98/95}$Mo values from 4 laboratories showed that the reproducibility of BCR-2 was consistent within ±0.06‰ (2SD), indicating the contamination mixed evenly with the original basalt. Therefore, it is difficult to consider that Mo isotopes in BCR-2 are not homogeneous based on only one data in Liu *et al.* (2016),[32] instead of presenting some comparable RMs such as BHVO-2 and SGR-1b.

3.5 Mo isotopes in geological and environmental reference materials

Besides the basalt BHVO-2 and BCR-2 mentioned above, the Mo isotope ratios in other igneous RMs, including GSR-3, GSR-2, AVG-2, GSP-2, and GSR-1, were also determined. Except that $\delta^{98/95}$Mo value (0.09 ± 0.012‰; $n = 3$) of GSR-1 has not been reported in previous studies (Table 3 and Fig. 5), the others are evidently identical to those published values[16,49] except for GSR-2, which has a ∼0.14‰ difference between the result we analyzed and reported by Zhao *et al.* (2016)[49] (Table 3). This observation implies that the Mo isotope composition of GSR-2 is possibly heterogeneous. The $\delta^{98/95}$Mo values of igneous rocks have a relatively large scan ranging from −1.73‰ to 0.59‰. The bulk silicate earth (BSE) and Phanerozoic upper crust have been limited to −0.15‰ or −0.21 ± 0.06‰ and ∼0.14 ± 0.07‰ (95%, SE), respectively.[6] In comparison with these values, our determined $\delta^{98/95}$Mo in igneous rock RMs are either similar to that of BSE or within the range of igneous rocks. Consequently, similar to BCR-2 and BHVO-2, GSR-3, AVG-2, and GSP-2 can also be used as the candidate RMs of the corresponding rocks for interlaboratory comparison.

Since carbonate rocks are expected to explore Mo isotope composition in coeval seawater or to restrict the minimum $\delta^{98/}$

^{95}Mo of seawater at any given time, Mo isotopes in carbonate have aroused the interest of some researchers in recent years.[10,20,52,53] However, there are few available Mo isotope data in carbonate RMs for laboratory comparison. The COQ-1 (carbonatite), GSR-6 (limestone), and JDO-1 (dolomite) are easily obtained from USGS and IGGE. The $\delta^{98/95}$Mo value of COQ-1 was -0.20 ± 0.01‰ (2SD, $n = 3$), indistinguishable from the published data (-0.26 ± 0.1‰, 2SD, $n = 5$) by Zhao *et al.* (2016).[49] However, GSR-6 (0.30 ± 0.02‰, 2SD, $n = 6$) had a ~0.21‰ difference from that (0.51 ± 0.9‰, 2SD, $n = 12$) reported by Liu *et al.* (2016).[32] This discrepancy is similar to the observation for BCR-2, which had a ~0.22‰ offset to those reported by other laboratories, indicating those reported values by Liu *et al.* (2016)[32] are likely to drift systematically at least 0.18‰ as suggested by Willbold *et al.* (2016).[30] The JDO-1 with 0.50 ± 0.02‰ (2SD, $n = 3$) of $\delta^{98/95}$Mo value was reported first. All these

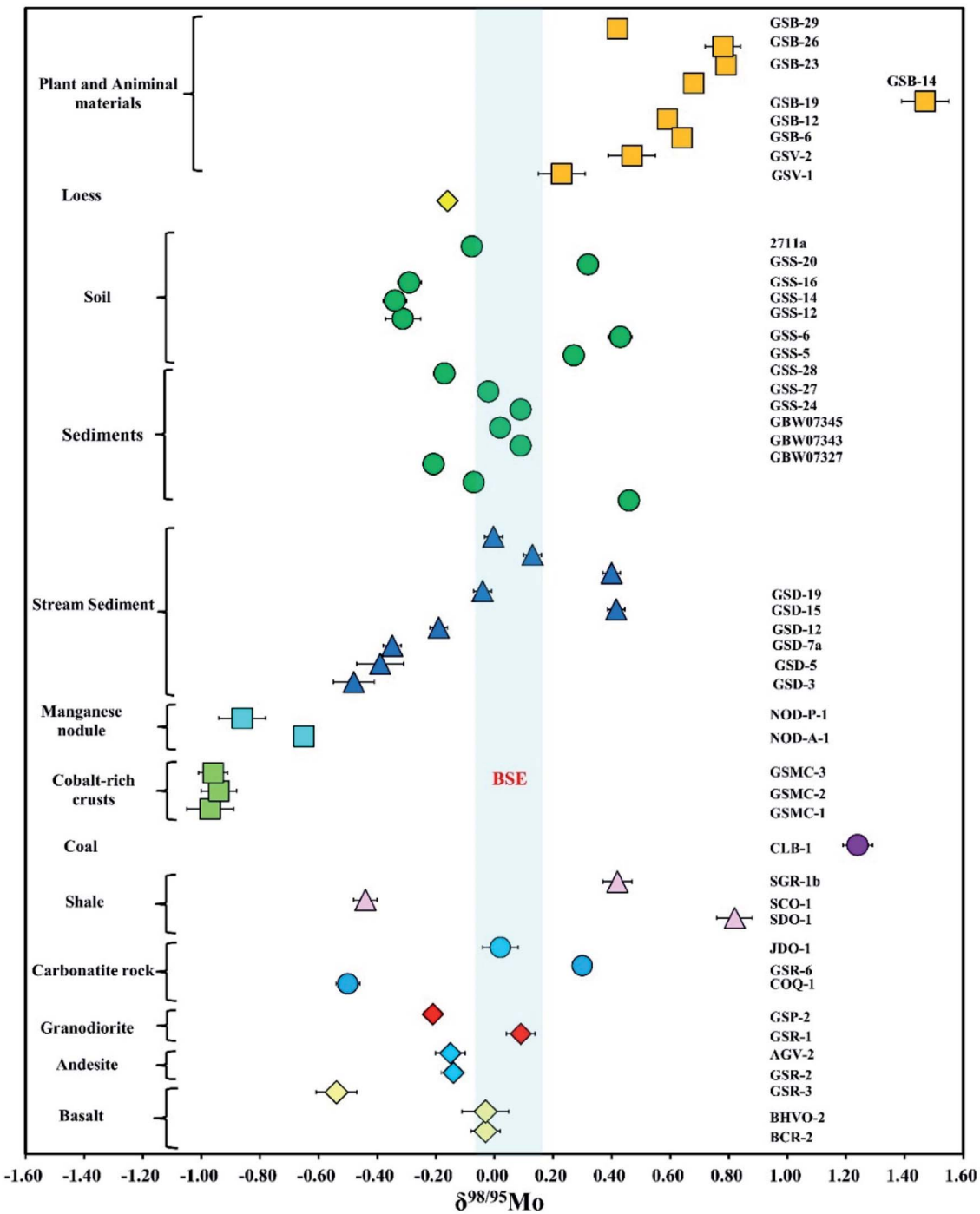

Fig. 5 Mo isotope compositions of geological and environmental reference materials determined in this study (BSE: bulk Silicate Earth, Greber *et al.* (2015)[15]).

carbonate $\delta^{98/95}$Mo values we measured are within the range of −1.79–2.10‰,[20,32,49,52,53] and most are smaller than that in seawater, consistent with the observation by Thoby *et al.* (2013).[52] Thus, these RMs can calibrate the Mo isotope composition of carbonates among different laboratories.

Mo isotopes in shales and organic-rich mudstones have been extensively employed to trace the evolution of redox and oxygen content in the paleo-ocean and atmosphere. Their isotope ratios vary significantly between ∼−1.00 to 2.10‰.[7–13] Two international shale RMs were determined to be 0.82 ± 0.05‰ (2SD, n = 4) for SDO-1 and −0.44 ± 0.04‰ (2SD, n = 4) for SCO-1 in this work, in great line with those reported in previous studies (Table 3). However, since SDO-1 and SCO-1 have been discontinued and are no longer available to most laboratories, the shale SGR-1b was also analyzed. To verify the Mo isotope homogeneity in different batches of SGR-1b, three lot. numbers, 0367, 0988, and 1005, were digested repeatedly. The $\delta^{98/95}$Mo were 0.43 ± 0.05‰ (2SD, n = 12) for 0367, 0.39 ± 0.03‰ (2SD, n = 9) for 0988 and 0.40 ± 0.03‰ (2SD, n = 6) for 1005. These values are excellently consistent with 0.44 ± 0.11‰ (2SD, n = 5) published by Zhao *et al.* (2016)[49] and 0.42 ± 0.02‰ (2SD, n = 3) reported by Li *et al.* (2016),[46] showing that the Mo isotope ratio of SGR-1bs is relatively homogeneous with $\delta^{98/95}$Mo of 0.41 ± 0.05‰ (2SD, n = 28). Therefore, we recommend that SGR-1b can be used as a substitute RM for interlaboratory comparison under the exhaustion of SDO-1 and SCO-1. Additionally, a CLB-1(coal R) was measured to be 1.25 ± 0.03‰ (2SD, n = 3), falling within the range of black shales.

Marine manganese nodules, ferromanganese and cobalt (Co)-rich crusts are potentially metalliferous mineral resources deposited on the seafloor. They have also been used as geological archives to reveal the evolution of element chemicals and their isotope compositions in seawater over time. The Mo isotopes of NOD-P-1 have been reported in the literature with homogeneous −0.86 ± 0.10‰, while the published $\delta^{98/95}$Mo of NOD-A-1 varied from −0.68 to −0.83‰ (Table 3). The value we measured was −0.65 ± 0.02‰, in accordance with the −0.68 ± 0.09‰ by Asael *et al.* (2013),[50], −0.66 ± 0.09‰ by Goto *et al.* (2015),[14], −0.73 ± 0.09‰ by Li *et al.* (2016)[46] and −0.70 ± 0.09‰ by Feng *et al.* (2020),[51] but slightly different from the −0.83 ± 0.09‰ by Zhao *et al.* (2016).[49] Given that the $\delta^{98/95}$Mo value reported by Barling *et al.* (2001)[7] is less accurate than the published results, the slight discrepancy of ≤0.19‰ between ours and Zhao *et al.* (2016)[49] might reflect the heterogeneity of Mo isotope composition in NOD-A-1. The $\delta^{98/95}$Mo values of three other Co-rich crust GSMC −1, −2 and −3 were −0.97 ± 0.05‰, −0.94 ± 0.05‰, and −0.96 ± 0.05‰, respectively. These results are identical with the Mo isotope composition of hydrogenous Fe–Mn crusts but different from the hydrothermal Mn nodules with a narrow range of −0.56‰ to −0.66‰.[14] Our results suggest that the Co-rich crust is also one of the potentially significant sinks of light Mo isotopes in seawater. Mo isotope composition in them can be used as an indicator to identify their origin.

Understanding Mo isotope systematics in loess, soils, and stream sediments is vital to exploring the biogeochemical cycle of Mo in the surficial environment. In this work, Mo isotope ratios of one loess, seven soils, and eighteen sediments taken from different provinces and river draining in metalliferous mine areas of China are reported (Table 3). The $\delta^{98/95}$Mo in loess (GSS-8) was −0.16 ± 0.03‰ (2SD, n = 3), slightly lighter than that average value (0.06 ± 0.15‰ with a range of −0.08 to 0.22‰, 2SD, n = 12) of loess from North China reported by Wang *et al.* (2018).[53] For soils, a polluted soil reference material NIST SRM 2711a was determined to be −0.08 ± 0.01‰ (2SD, n = 3). The others varied from −0.29 to 0.43‰ with an average value of 0.01 ± 0.36‰ (1SD, n = 6), heavier than those soils (an average was −0.23 ± 0.16‰ (2SD, n = 4)) from the strongly weathered profile of granite and igneous bedrock. However, these $\delta^{98/95}$Mo values still fall within the range of −0.41–1.5‰, which interpreted this observation as being controlled by redox conditions, organic matter, and atmosphere inputs.[54–58] The $\delta^{98/95}$Mo of eighteen sediments ranges from −0.48‰ to 0.46‰ with an average value of 0.03 ± 0.27‰ (1SD, n = 18), slightly lighter than that in loess from North China and upper continent crust (0.05–0.15‰),[59–61] But its variation coefficient is large, different from the relatively homogenous Ni and Cr isotopes.[30,62] This observation suggests that Mo isotope composition in these sediments is heterogeneous, reflecting the impact of various environmental factors demonstrated by Siebert *et al.* (2015).[55]

The $\delta^{98/95}$Mo values of eight plant RMs are reported for the first time (Table 3), varying from 0.23‰ to 0.79‰ except for GSB-14 (seaweed) having a $\delta^{98/95}$Mo (1.47 ± 0.04‰, n = 4) close to the seawater (2.06 ± 0.06‰). Their average was 0.60‰ ± 0.20‰ (n = 7, 1SD), higher than that in soil, sediment, and rock samples (Fig. 5). This observation is similar to the finding by Malinovsky *et al.* (2018),[27] whose work showed that plant roots generally enriched heavier Mo isotopes but different from the isotopes of K, Ca in plants,[63] which are lighter in comparison with rock samples. The relatively positive $\delta^{98/95}$Mo in plants, as demonstrated by Malinovsky *et al.* (2018),[27] indicates that MoO_4^{2-} with heavier isotopes prefers to be uptaken by plant root cells from soils. Additionally, GSB-29, a swine liver, is 0.42 ± 0.03‰ (2SD, n = 4), obviously contrary to the Cd isotopes with the lighter isotopic composition,[37] which implies that Mo isotope composition in animal tissues may be related to the Mo speciation in the food chain. However, this still needs more work to verify. Overall, these results exhibit Mo isotopes have great potential in studying Mo biochemistry and environmental chemistry.

4. Conclusions

In order to analyze the $\delta^{98/95}$Mo values of lower Mo geological and environmental samples with complex matrices, an improved Mo purification and cleaning resin scheme was proposed using commercially available Muromac®1X8 anion and AG50-X8 cation resins. The samples containing 30–60 ng Mo can be used to extract Mo for isotope measurement. The total blank of Mo from sample digestion to Mo separation is decreased to 0.16 ng. Attribute to good separation, interference elements (Zr, Fe, Zn, and Sn), and matrix effects can be efficiently removed even for samples with the ratio of [Fe]/[Mo] as high as 80 000.

The Mo isotope measurement with high sensitivity (200–330 V μg^{-1} mL) can be achieved using an improved Aridus II with an ice chamber in the sample introduction system. When the sensitivity of the ^{95}Mo signal increases, Mo isotopes can be determined with the typically external precision of ≤0.06‰ at the injecting concentration of 5–10 ng mL^{-1}. The isotopic measurement of the international GRMs, such as BHVO-2 (−0.03 ± 0.05‰), AGV-2 (−0.15 ± 0.02‰), SGR-1b (0.42 ± 0.03‰), SDO-1 (0.82 ± 0.05‰), NOD-A-1 (−0.65 ± 0.02‰), and NOD-P-1 (−0.86 ± 0.03‰), are consistent with the $\delta^{98/95}$Mo values published by previous studies, confirming that the high-precision measurement of Mo isotopes can be conducted at the 5 ng level using double spike MC-ICP-MS.

Besides the GRMs aforementioned, other 43 RMs, including granodiorite, Co-rich crusts, coal, soil, stream sediments, and organisms, are reported for the first time. GSR-3, GSP-2, SGR-1b, JDO-1, GSR-6, and others with obviously positive or negative $\delta^{98/95}$Mo values could be used as a substitute under the exhaustion of corresponding RMs, and as a criterion for intercalibration among different laboratories in the future. In summary, Mo isotope measurements of a broader range of RMs, even with low Mo concentration and complex matrix, are applicable at 5 ng levels under a high-sensitivity setup with robust accuracy and precision. This will further expand the application of Mo isotopes in high-temperature geochemistry and extend in multiple research areas.

Author contributions

H.-G. Z. and J.-M. Z. did writing – review & editing and visualization; J.-M. Z. made conceptualization, data curation, funding acquisition, resources and investigation; J.-M. Z. and D. T. designed methodology; D. T. and X. L. did some visualization; X. L., K. L. and W. Y. conducted investigation; J.-M. Z. did project administration and supervision. All authors contributed to the discussion and revision of the manuscript.

Conflicts of interest

There are no conflicts to declare.

Acknowledgements

This work was financially supported by the National Key R&D Program of China (2019YFA0708400) and the National Natural Science Foundation of China (No. U1612441, 41073017). We are grateful to Dr Yuyang He and Mr Guangliang Wu for the help of polishing English and figure rendering. Drs Xiang-Kun Zhu and Jin Li are greatly appreciated for providing NIST SRM 3134 (lot. 891307). We also appreciate two anonymous reviewers' constructive comments and insightful suggestions to improve the paper quality.

References

1 A. J. Mayer and M. E. Wieser, *J. Anal. At. Spectrom.*, 2014, **29**, 85–94.
2 C. Scott and T. W. Lyons, *Chem. Geol.*, 2012, **324**, 19–27.
3 D. Malinovsky, H. Dan, B. Ilyashuk, O. Martinsson and J. Gelting, *Chem. Geol.*, 2007, **236**, 181–198.
4 C. Archer and D. Vance, *Nat. Geosci.*, 2008, **1**, 597–600.
5 C. R. Pearce, K. W. Burton, P. Strandmann, R. H. James and S. Gíslason, *Earth Planet. Sci. Lett.*, 2010, **295**, 104–114.
6 B. Kendall, T. W. Dahl, A. D. Anbar and G. Golly, *Non-Traditional Stable Isotopes*, Mineralogical Soc Amer & Geochemical Soc, Chantilly, 2017, pp. 683–732.
7 J. Barling, G. L. Arnold and A. D. Anbar, *Earth Planet. Sci. Lett.*, 2001, **193**, 447–457.
8 C. Siebert, T. F. Nägler, F. von Blanckenburg and J. D. Kramers, *Earth Planet. Sci. Lett.*, 2003, **211**, 159–171.
9 G. L. Arnold, A. D. Anbar, J. Barling and T. W. Lyons, *Science*, 2004, **304**, 87–90.
10 A. R. Voegelin, T. F. N. Gler, E. Samankassou and I. M. Villa, *Chem. Geol.*, 2009, **265**, 488–498.
11 H. J. Wen, J. Carignan, Y. X. Zhang, H. F. Fan, C. Cloquet and S. R. Liu, *Geology*, 2011, **39**, 775–778.
12 G. J. Baldwin, T. F. Nägler, N. D. Greber, E. C. Turner and B. S. Kamber, *Precambrian Res.*, 2013, **230**, 168–178.
13 N. J. Planavsky, D. Asael, A. Hofmann, C. T. Reinhard, S. V. Lalonde, A. Knudsen, X. Wang, F. O. Ossa, E. Pecoits and A. Smith, *Nat. Geosci.*, 2014, **7**, 283–286.
14 K. T. Goto, G. Shimoda, A. D. Anbar, G. W. Gordon, Y. Harigane, R. Senda and K. Suzuki, *Mar. Geol.*, 2015, **369**, 91–99.
15 N. D. Greber, I. S. Puchtel, T. Nägler and K. Mezger, *Earth Planet. Sci. Lett.*, 2015, **421**, 129–138.
16 J. Yang, C. Siebert, J. Barling, P. Savage, Y. H. Liang and A. N. Halliday, *Geochim. Cosmochim. Acta*, 2015, **162**, 126–136.
17 S. KöNig, M. Wille, A. Voegelin and R. Schoenberg, *Earth Planet. Sci. Lett.*, 2016, **447**, 95–102.
18 S. Chen, R. C. Hin, T. John, R. Brooker, B. Bryan, Y. Niu and T. Elliott, *Nat. Commun.*, 2019, **10**, 4773, DOI: 10.1038/s41467-019-12696-3.
19 H. Y. Li, J. Li, J. G. Ryan, X. Li and Y. G. Xu, *Earth Planet. Sci. Lett.*, 2019, **520**, 105–114.
20 Y. Zhang, C. Yuan, M. Sun, J. Li, X. Long, Y. Jiang and Z. Huang, *Geochim. Cosmochim. Acta*, 2020, **278**, 340–352.
21 R. Bezard, M. Fischer-Godde, C. Hamelin, G. A. Brennecka and T. Kleine, *Earth Planet. Sci. Lett.*, 2016, **453**, 171–181.
22 H. Freymuth, F. Vils, M. Willbold, R. N. Taylor and T. Elliott, *Earth Planet. Sci. Lett.*, 2015, **432**, 176–186.
23 C. Burkhardt, R. C. Hin, T. Kleine and B. Bourdon, *Earth Planet. Sci. Lett.*, 2014, **391**, 201–211.
24 H. Freymuth, T. Elliott, M. van Soest and S. Skora, *Geology*, 2016, **44**, 987–990.
25 Y. Wang, L. Zhou, S. Gao, J. W. Li, Z. F. Hu, L. Yang and Z. C. Hu, *Miner. Deposita*, 2016, **51**, 201–210.
26 B. N. Kaiser, K. L. Gridley, J. N. Brady, T. Phillips and S. D. Tyerman, *Ann. Bot.*, 2005, **96**, 745–754.
27 D. Malinovsky and N. A. Kashulin, *Anal. Methods*, 2018, **10**, 131–137.

28 J. J. Fan, J. Li, Q. Wang, L. Zhang, J. Zhang, X. L. Zeng, L. Ma and Z. L. Wang, *Chem. Geol.*, 2020, **545**, 119648, DOI: 10.1016/j.chemgeo.2020.119648.
29 R. Hansch and R. R. Mendel, *Curr. Opin. Plant Biol.*, 2009, **12**, 259–266.
30 M. Willbold, K. Hibbert, Y. J. Lai, H. Freymuth, R. C. Hin, C. Coath, F. Vils and T. Elliott, *Geostand. Geoanal. Res.*, 2016, **40**, 389–403.
31 N. D. Greber, C. Siebert, T. F. Nägler and T. Pettke, *Geostand. Geoanal. Res.*, 2012, **36**, 291–300.
32 J. Liu, H. Wen, H. Fan, C. Zhu and Y. Zhang, *J. Anal. At. Spectrom.*, 2016, **31**, 1287–1297.
33 Y. H. Liang, A. N. Halliday, C. Siebert, J. G. Fitton, K. W. Burton, K. L. Wang and J. Harvey, *Geochim. Cosmochim. Acta*, 2017, **199**, 91–111.
34 J. Li, X. R. Liang, L. F. Zhong, X. C. Wang, Z. Y. Ren, S. L. Sun, Z. F. Zhang and J. F. Xu, *Geostand. Geoanal. Res.*, 2014, **38**, 345–354.
35 N. Gaspers, T. Magna and L. Ackerman, *Geostand. Geoanal. Res.*, 2020, **44**, 363–374.
36 J. M. Zhu, G. Wu, X. Wang, G. Han and L. Zhang, *J. Anal. At. Spectrom.*, 2018, **33**, 809–821.
37 D. Tan, J. M. Zhu, X. Wang, G. Han and W. Xu, *J. Anal. At. Spectrom.*, 2020, **35**, 713–727.
38 A. J. Pietruszka, R. J. Walker and P. A. Candela, *Chem. Geol.*, 2006, **225**, 121–136.
39 C. Siebert, T. F. Nägler and J. D. Kramers, *Geochem., Geophys., Geosyst.*, 2001, **2**(7), 1032–1047.
40 S. G. John, *J. Anal. At. Spectrom.*, 2012, **27**, 2123–2131.
41 E. K. Skierszkan, M. Amini and D. Weis, *Anal. Bioanal. Chem.*, 2015, **407**, 1925–1935.
42 J. M. Zhu, D. C. Tan and J. Wang, *Acta Petrol. Sin.*, 2018, **34**, 503–512, in Chinese with English abstract.
43 H. Wen, J. Carignan, C. Cloquet, X. Zhu and Y. Zhang, *J. Anal. At. Spectrom.*, 2010, **25**, 716–721.
44 T. Goldberg, G. Gordon, G. Izon, C. Archer, C. R. Pearce, J. McManus, A. D. Anbar and M. Rehkamper, *J. Anal. At. Spectrom.*, 2013, **28**, 724–735.
45 T. F. Nägler, A. D. Anbar, C. Archer, T. Goldberg, G. W. Gordon, N. D. Greber, C. Siebert, Y. Sohrin and D. Vance, *Geostand. Geoanal. Res.*, 2014, **38**, 149–151.
46 J. Li, X.-k. Zhu, S.-h. Tang and K. Zhang, *Geostand. Geoanal. Res.*, 2016, **40**, 405–415.
47 A. R. Voegelin, T. F. Nägler, E. Samankassou and I. M. Villa, *Chem. Geol.*, 2009, **265**, 488–498.
48 G. Wu, J. M. Zhu, X. Wang, T. M. Johnson and G. Han, *Anal. Chem.*, 2019, **92**, 1463–1469.
49 P. Zhao, J. Li, L. Zhang, Z. Wang, D. Kong, J. Ma, G. Wei and J. Xu, *Geostand. Geoanal. Res.*, 2016, **40**, 217–226.
50 D. Asael, F. L. H. Tissot, C. T. Reinhard, O. Rouxel, N. Dauphas, T. W. Lyons, E. Ponzevera, C. Liorzou and S. Cheron, *Chem. Geol.*, 2013, **362**, 193–210.
51 L. P. Feng, L. Zhou, W. F. Hu, W. Zhang, B. C. Li, Y. S. Liu, Z. C. Hu and L. Yang, *J. Anal. At. Spectrom.*, 2020, **35**, 145–154.
52 M. Thoby, K. O. Konhauser, P. W. Fralick, W. Altermann, P. T. Visscher and S. V. Lalonde, *Geology*, 2019, **47**, 559–562.
53 Z. B. Wang, J. Li, G. J. Wei, W. F. Deng, X. F. Chen, T. Zeng, X. J. Wang, J. L. Ma, L. Zhang, X. L. Tu, Q. Wang and M. McCulloch, *Geochim. Cosmochim. Acta*, 2019, **262**, 128–142.
54 Z. B. Wang, J. L. Ma, J. Li, G. J. Wei, T. Zeng, L. Li, L. Zhang, W. F. Deng, L. H. Xie and Z. F. Liu, *Geochim. Cosmochim. Acta*, 2018, **226**, 1–17.
55 C. Siebert, J. C. Pett-Ridge, S. Opfergelt, R. A. Guicharnaud, A. N. Halliday and K. W. Burton, *Geochim. Cosmochim. Acta*, 2015, **162**, 1–24.
56 E. K. King, S. S. Perakis and J. C. Pett-Ridge, *Geochim. Cosmochim. Acta*, 2018, **222**, 584–598.
57 E. K. King, A. Thompson, O. A. Chadwick and J. C. Pett-Ridge, *Chem. Geol.*, 2016, **445**, 54–67.
58 Z. B. Wang, J. L. Ma, J. Li, T. Zeng, Z. Y. Zhang, X. Y. He, L. Zhang and G. J. Wei, *Geochim. Cosmochim. Acta*, 2020, **286**, 380–403.
59 J. Yang, J. Barling, C. Siebert, J. Fietzke, E. Stephens and A. N. Halliday, *Geochim. Cosmochim. Acta*, 2017, **205**, 168–186.
60 A. R. Voegelin, T. Pettke, N. D. Greber, B. von Niederhausern and T. F. Nagler, *Lithos*, 2014, **190**, 440–448.
61 M. Willbold and T. Elliott, *Chem. Geol.*, 2017, **449**, 253–268.
62 G. Wu, J. M. Zhu, X. Wang, G. Han, D. Tan and S. J. Wang, *J. Anal. At. Spectrom.*, 2019, **34**, 1639–1651.
63 J. N. Christensen, L. P. Qin, S. T. Brown and D. J. DePaolo, *ACS Earth Space Chem.*, 2018, **2**, 745–752.
64 V. Migeon, B. Bourdon, E. Pili and C. Fitoussi, *J. Anal. At. Spectrom.*, 2015, **30**, 1988–1996.